Chapter 6

Solution Mechanisms for Dopant Oxides in Yttria

The work presented in this chapter has been published in the Journal of the American Ceramics Society [20]. Since the atomistic simulation methodology has been described in detail in chapter 2, these details have been omitted here.

6.1 Introduction

Due to the very high Schottky and Frenkel formation energies in high melting point oxides, the transport of ions through these materials is controlled by their impurity content. Consequently explanations of experimental data based on simple point defect compensation mechanisms have become well established in recent ceramics literature [116–119]. However, such models do not generally consider the possibility of defect cluster formation and usually assume only one type of dopant ion to be responsible for controlling ion transport.

Recent work by Chen and Chen [116] has shown that in Y_2O_3 different dopants have dramatically different effects on grain growth. Analysis of these results, based on defect models, led to the conclusion that impurities must be exhibiting unusually strong binding energies to point defects. Furthermore, it was suggested that this was a consequence of the low dielectric constant of Y_2O_3 .

To understand some of the reasons why different dopant ions have such different effects, it would be of great interest to carry out a systematic study of dopant energetics, including solution mechanisms and defect cluster formation. Of course, this is an onerous task since the defect energies involved are often high and the experimental data are correspondingly difficult to determine. As such, atomistic computer simulation techniques are an attractive alternative, particularly when considering a series of dopants where one need only focus on the relative energies rather than the absolute predicted energetics.

Here we shall consider the effect of doping a host Y_2O_3 lattice with a range of aliovalent and isovalent cations. The results will be analysed as a function of cation radius. The aim is to determine if solution compensation mechanisms change with ion size and if so, whether it is possible to identify a trend.

6.1.1 Crystallography

Yttria exhibits the cubic bixbyite structure ($Ia3$, No. 206) with a lattice parameter of 10.604 Å [120]. All oxygen ions occupy distorted four coordinate 48e positions. The Y^{3+} ions occupy two different sites, 8a and 24d, although both of these sites are distorted 6 coordinate.

As a consequence, there will be a single oxygen vacancy energy ($V_O^{\bullet\bullet}$) but two different Y^{3+} vacancy energies ($V_Y^{'''}$).

Y_2O_3 interstitial sites.		
	Nearest neigbours	
Site	Cation	Anion
8*b*	6	6
16*c*	4	6
24*d*	6	6

Table 6.1: Properties of interstitial sites in Y_2O_3. Although the 8*b* and 24*d* sites share the same number of cation and anion neighbours, they are both distorted from an ideal octahedron in different ways.

The bixbyite structure can accommodate interstitial ions at three distinctly different sites: the 8*b* position, the 16*c* (x=$\frac{1}{8}$) position and the 24*d* (x=-$\frac{1}{4}$) position. The 8*b* and 24*d* interstitial sites are associated with the two types of cation positions. Table 6.1 summarizes the differences between these three sites.

6.1.2 Solution mechanisms

Solution of isovalent ions occurs via a simple substitution reaction (see section 6.3.2). However, the solution of aliovalent oxides can occur in a number of different ways, all of which involve the formation of charge compensating defects. In the case of A^{2+} substitution, the neutrality condition can be met by assuming cation interstitials ($A_i^{\bullet\bullet}$ or $Y_i^{\bullet\bullet\bullet}$) or anion vacancies ($V_O^{\bullet\bullet}$). For M^{4+} dopant cations, the charge compensating species will be cation vacancies ($V_Y^{\prime\prime\prime}$) or oxygen interstitial ions ($O_i^{\prime\prime}$). Additionally, the clustering of dopant ions and their charge compensating defects can reduce solution enthalpies significantly [44]. In the complex structure that Y_2O_3 exhibits, it is possible to form clusters of various charges and geometries. All would

need to be considered if the calculated defect enthalpies were to be used to predict the solution equilibria associated with the accomodation of a dopant type. However, here we will restrict ourselves to calculating only solution via isolated point defects and via neutral defect clusters and use this data to illustrate that defect clustering is important in this system.

We choose not to consider charge compensation via electronic defects (i.e. holes or electrons) or by protons. Protons have been shown to be the important charge compensating defects for Mg and Ca doped Y_2O_3 unless the water vapour pressure is kept sufficiently low [121, 122]. In dry conditions, these experimental results suggested that oxygen vacancies become the dominant charge compensating defects rather than electronic holes. The present study therefore relates primarily to dry Y_2O_3 .

In all cases, the individual component defect enthalpies are calculated using the methodology outlined below. These calculated solution enthalpies are then used as the basis for understanding the defect behaviour in this material. For example, it is possible to carry out mass action calculations using the calculated enthalpies to predict the equilibrium solution limits of impurity content [123]. However, the computational method we have employed is approximate. As such, rather than use the absolute predicted enthalpies, in this study we shall focus on issues that concern the differences in predicted enthalpies: in particular, the most energetically favourable solution mechanism.

When calculating defect binding enthalpies, we will use the following definition;

$$E_{\text{binding}} = \left(\sum_{\text{components}} E(\text{point defects}) \right) - E(\text{defect cluster}) \qquad (6.1)$$

so that a positive binding enthalpy implies that the defect cluster is stable with respect to its constituent point defect components.

6.2 Methodology

The simulation methodology has been described in detail in chapter 2. The inter ionic potential and the shell model parameters and their source are presented in Table 6.2 and 6.3.

6.3 Results

6.3.1 Basic Lattice Properties

Before simulating the effect of dopants in Y_2O_3 it is necessary to simulate the properties of the perfect lattice. Table 6.4 shows the simulated values; the lattice parameter, the elastic properties, the dielectric properties and the intrinsic defect reaction enthalpies. The lattice parameter is reproduced to within 0.06% of the experimental value (which corresponds with a 0.1% error in the unit cell volume).

Ünal and Akinc report an elastic modulus of 150 GN/m^2 [125] for a polycrystalline material. Previous experiments report 57–177 GN/m^2 [126] and 170 GN/m^2 [127]. The predicted elastic constants of Table 6.4 would yield an elastic modulus of 187 GN/m^2 but, of course, this predicted value corresponds to an average for a single crystal. Therefore, the calculated value is clearly reasonable. Both the static and the high-frequency dielectric constants predicted for the material are exceptionally low for a ceramic. However, these are consistent with the values reported in literature [116].

The oxygen Frenkel reaction is predicted to be the dominant intrinsic disorder reaction (see Table 6.4). This is a consequence of the relatively open bixbyite structure. The Frenkel energy was evaluated using the 16*c* interstitial site. The 8*b* and

Buckingham inter-atomic potential parameters				
Interaction	A [eV]	ρ [Å]	C [eV Å^6]	reference
O^{2-} – O^{2-}	9547.96	0.21916	32.0	[101]
Mg^{2+} – O^{2-}	1284.38	0.29969	0.0	[124]
Zn^{2+} – O^{2-}	529.70	0.3581	0.0	[101]
Cd^{2+} – O^{2-}	951.88	0.34856	13.91	
Ca^{2+} – O^{2-}	784.38	0.36356	0.0	
Sr^{2+} – O^{2-}	682.17	0.3945	0.0	[25]
Ba^{2+} – O^{2-}	905.7	0.3976	0.0	
Al^{3+} – O^{2-}	1725.20	0.28971	0.00	[124]
Cr^{3+} – O^{2-}	1204.18	0.31650	0.00	[101]
Sc^{3+} – O^{2-}	1575.85	0.32110	0.00	
Y^{3+} – O^{2-}	1766.40	0.33849	19.43	[44]
In^{3+} – O^{2-}	1495.65	0.33272	0.00	[26]
Gd^{3+} – O^{2-}	1885.75	0.3399	20.34	
La^{3+} – O^{2-}	1968.92	0.34600	0.00	
Ti^{4+} – O^{2-}	2179.122	0.30384	8.986	[25]
Zr^{4+} – O^{2-}	1234.73	0.358	0.0	
Ce^{4+} – O^{2-}	1809.68	0.3547	20.4	
U^{4+} – O^{2-}	1761.775	0.356421	0.0	

Table 6.2: Buckingham potential parameters (see equation 2.51).

Shell model parameters		
Ion	Shell charge [e]	k [eVÅ^{-2}]
O^{2-}	-2.04	6.3
In^{3+}	-6.1	1680.0
Ti^{4+}	-0.1	200.0
Ce^{4+}	-0.2	177.84
U^{4+}	-0.1	160.0

Table 6.3: Shell model parameters.

Predicted Lattice properties		
Lattice parameter:	10.598	Å
Elastic constants:		
ϵ_{11}	274.34	GNm^{-2}
ϵ_{12}	132.65	GNm^{-2}
ϵ_{44}	107.79	GNm^{-2}
Relative dielectric constants:		
ϵ^0	5.88	
ϵ^∞	3.67	
Intrinsic defect reaction enthalpies		
Anion Frenkel	4.05	eV/defect
Cation Frenkel	8.73	eV/defect
Schottky	5.65	eV/defect
Lattice Energy	-135.498	eV/unit cell

Table 6.4: Predicted Y_2O_3 lattice properties.

24*c* oxygen interstitial sites yield defect enthalpies 1.7 and 3.0 eV higher than the 16*c* site. Clearly the selection of the correct (ie. lowest energy) interstitial site is important in this structure.

6.3.2 Isovalent Oxides

Solution of the isovalent ions, Al^{3+}, Cr^{3+}, Sc^{3+}, In^{3+}, Gd^{3+} and La^{3+}, in yttria, occurs via a simple substitution reaction (using Kröger-Vink notation):

$$M_2O_3 + 2Y_Y^{\times} \rightleftharpoons 2M_Y^{\times} + Y_2O_{3(s)}. \tag{6.2}$$

For reaction (6.2) we need to perform two defect calculations per substitutional ion, as there are two distinct cation lattice sites.

In addition we need to calculate the cohesive energies of both host and dopant lattice. These lattice energies have been calculated as described in section 2.2. The predicted lattice parameters match closely if not exactly the experimental values as can be seen in Table 6.5. An exception is Cr_2O_3, where the predicted lattice volume is too small. The potential used was derived for the study of chromate spinel and has not been properly fitted with other structures.

The resulting solution enthalpies are plotted against the ionic radii [105] of the dopant (solute) ion, in Figure 6.1. Both the 8*a* and the 24*d* lattice site substitutions were simulated, and the figure shows a slight difference in solution enthalpies in favour of the 24*d* sites for ions smaller than Y^{3+} but the 8*a* site for ions larger than Y^{3+}.

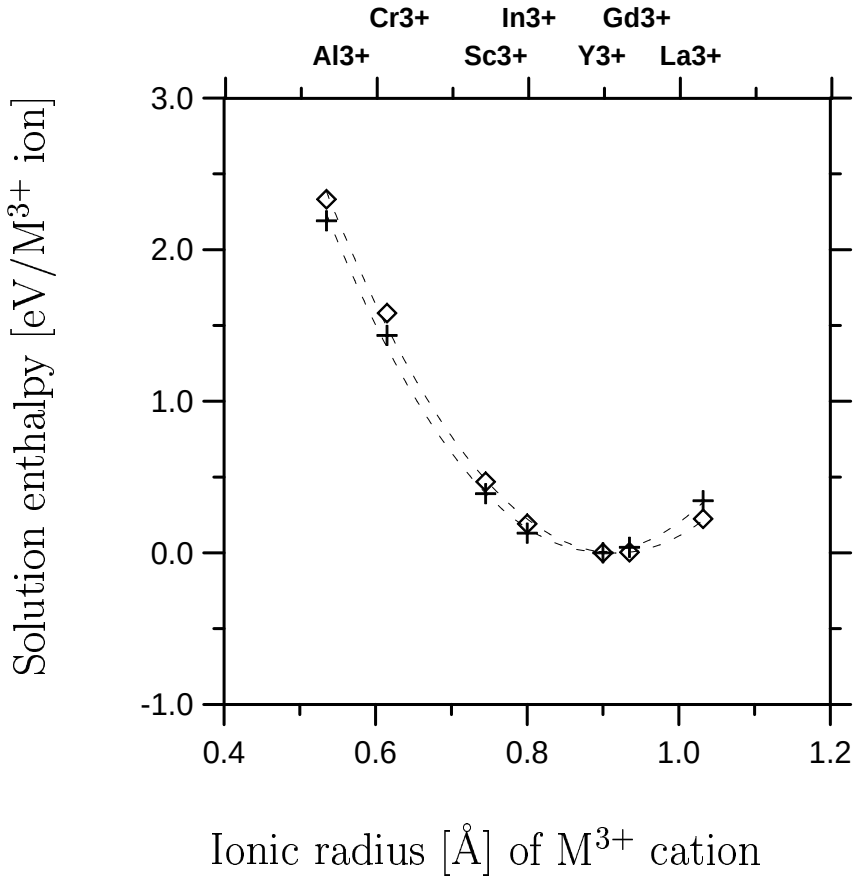

Figure 6.1: Enthalpy of solution of isovalent oxide ([eV/M^{3+}]) in Y_2O_3. The 8*a* and 24*d* sites are indicated with a "$\diamond$" and a "+" respectively.

Crystal	Unit cell volume [Å^2]		Lattice energy
	Literature	Simulation	[eV per formula unit]
Al_2O_3	255.45	255.45	161.140
Cr_2O_3	288.716	276.807	155.047
Sc_2O_3	954.22	953.51	145.309
In_2O_3	1035.82	1036.25	141.109
Gd_2O_3	1192.37	1261.22	133.245
La_2O_3	82.30	82.31	127.167

Table 6.5: Experimental and predicted lattice volumes and lattice energies of M_2O_3 type ceramics. The predicted lattice volumes are accurate except for Cr_2O_3.

6.3.3 Solution mechanisms for monoxides

The solution of monoxides into yttria requires the formation of a charge compensating intrinsic defect. Let us consider, initially, the infinite dilution limit where solution of these A^{2+} ions occurs without the formation of clusters. Under these circumstances charge compensation can be achieved via three different mechanisms:

$$I. \quad AO_{(s)} \overset{Y_2O_3}{\rightarrow} \frac{2}{3}A'_Y + \frac{1}{3}A_i^{\bullet\bullet} + \frac{1}{3}Y_2O_{3(s)}$$

$$II. \quad AO_{(s)} \overset{Y_2O_3}{\rightarrow} A'_Y + \frac{1}{2}V_O^{\bullet\bullet} + \frac{1}{2}Y_2O_{3(s)}$$

$$III. \quad AO_{(s)} \overset{Y_2O_3}{\rightarrow} A'_Y + \frac{1}{3}Y_i^{\bullet\bullet\bullet} + \frac{1}{3}Y_2O_{3(s)}$$

We have simulated the metal interstitial defects and the substitutional defects at all symmetry sites available in the crystal. The lowest energy solution site depends on which ion is being considered. Mg^{2+} and Zn^{2+} prefer to occupy $24d$ interstitial

Neutral cluster binding energies			
	Reaction energy [eV]		
Solute	$\{2A'_Y : A_i^{\bullet\bullet}\}^\times$	$\{2A'_Y : V_O^{\bullet\bullet}\}^\times$	$\{3A'_Y : Y_i^{\bullet\bullet\bullet}\}^\times$
MgO	3.771	4.383	10.006
ZnO	3.826	4.364	9.777
CdO	3.900	3.613	7.848
CaO	3.854	3.534	7.384
SrO	3.823	3.344	6.043
BaO	3.348	3.170	4.479

Table 6.6: The total binding energy (i.e. *not* per defect) of neutral defect clusters incorporating A^{2+} solute ions for the three solution mechanisms.

sites, whereas ions with a larger radius will occupy 16*c* sites. The solution enthalpy difference between occupation of the two sites is only a few tenths of an electron Volt.

Figure 6.2 shows the solution enthalpies, for one AO formula unit (i.e. eV/AO), for the three monoxide reactions as a function of ion radius. It is clear that the dopant interstitial compensating reaction (I) is the most favourable, if we assume that defects are spatially isolated from each other.

The formation of defect clusters, and in particular, neutral defect clusters, decreases the solution enthalpy considerably. Reactions I, II and III can generate the formation of $\{A'_Y : A_i^{\bullet\bullet} : A'_Y\}^\times$, $\{A'_Y : V_O^{\bullet\bullet} : A'_Y\}^\times$ and $\{A'_Y : A'_Y : Y_i^{\bullet\bullet\bullet} : A'_Y\}^\times$ clusters respectively. The binding energies for these clusters (see Table 6.6) are comparable with the respective solution enthalpies. Furthermore, when defect clustering is included, the preferred solution mechanism can be different (see Figure 6.3)

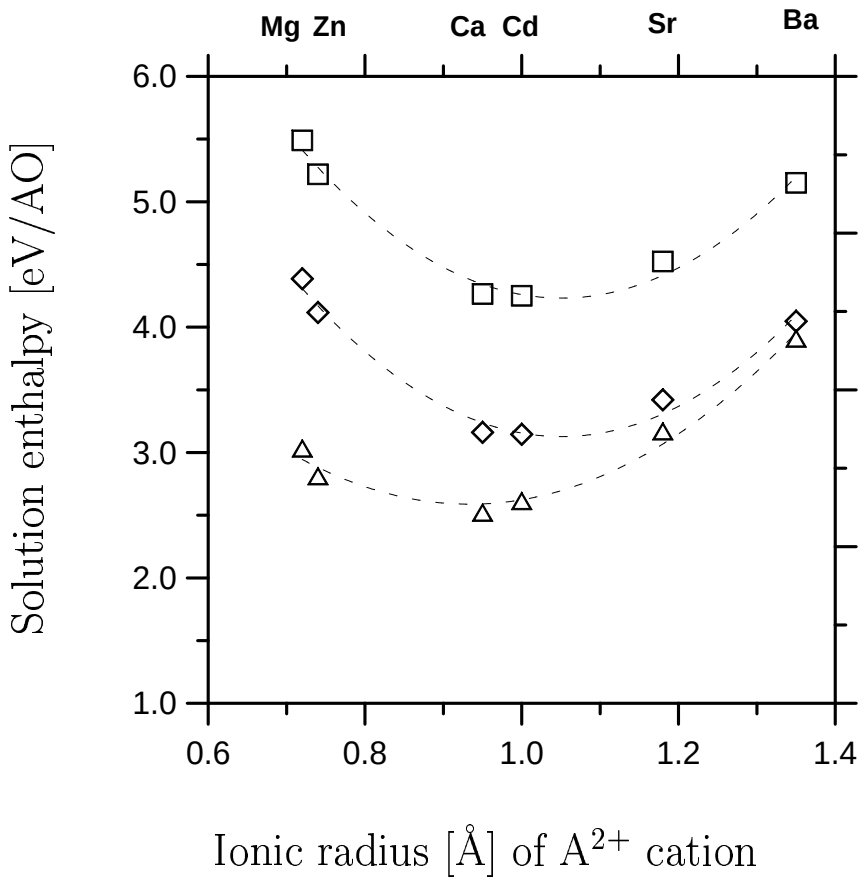

Figure 6.2: Enthalpy of solution of AO oxides in Y_2O_3 assuming that isolated defects form. The three solution mechanisms shown here are dopant interstitial compensating reaction (I) (indicated with a Δ), oxygen vacancy compensated reaction ($\diamond$) and yttrium interstitial compensated reaction ($\square$). Not all interstitial and substitutional ions occupy the same lattice sites: Mg^{2+} and Zn^{2+} ions occupy 24*d* interstitial sites and 16c substitutional sites, whereas the larger ions occupy 16*c* interstitial sites and 8*a* substitutional sites.

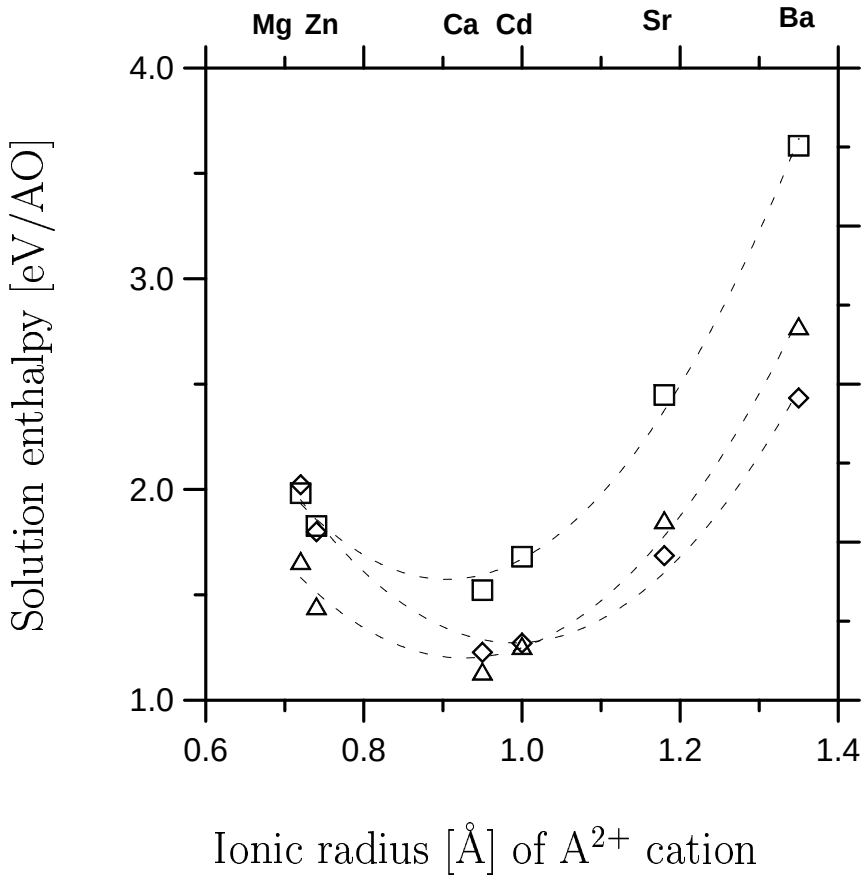

Figure 6.3: Enthalpy of solution of AO oxides in Y_2O_3 assuming defects form neutral clusters. The self compensating solution mechanism ("Δ", formation of $\{2A'_Y : A_i^{\bullet\bullet}\}^{\times}$ clusters) is predicted to be dominant at A^{2+} radii smaller than 1Å. For radii greater than 1Å, oxygen vacancy compensated clusters ("$\diamond$", $\{2A'_Y : V_O^{\bullet\bullet}\}^{\times}$) have the lowest solution enthalpy. Yttrium interstitial compensated clusters are indicated with a "$\square$".

from that predicted with the isolated defect model (ie. in Figure 6.2). Indeed, Figure 6.3 shows that there is a crossover in the preferred solution mechanism from dopant interstitial compensation (reaction I) to oxygen vacancy (reaction II) compensation.

It is interesting to note that the total binding energies reported in Table 6.6 are exceptionally large compared to, for example, those found in related materials such as Al_2O_3 (compare for example to Table XI in reference [124]). This is due primarily to the very low dielectric constant of the Y_2O_3 lattice.

The binding energies (see Table 6.6) associated with the yttrium-interstitial compensation reactions (reaction III) are much higher than the corresponding binding energies for clusters associated with reactions I and II. Nevertheless, the solution enthalpies for reaction III, assuming defect cluster formation, are still larger than those associated with reactions I and II, assuming defect cluster formation. (Note: the binding energies in Table 6.6 are for a complete cluster whereas reactions I, II and III result in the formation of only part of a cluster.)

6.3.4 Solution mechanisms for dioxides

The solution of dioxides relies on the formation of either an oxygen interstitial or a yttrium vacancy as the charge compensating species. As with monoxide solution, we first investigate the solution behaviour assuming spatially isolated defects.

$$I. \qquad BO_{2(s)} \overset{Y_2O_3}{\rightarrow} B_Y^{\bullet} + \frac{1}{2}O_i'' + \frac{1}{2}Y_2O_{3(s)}$$

$$II. \qquad BO_{2(s)} \overset{Y_2O_3}{\rightarrow} B_Y^{\bullet} + \frac{1}{3}V_Y''' + \frac{2}{3}Y_2O_{3(s)}$$

The results, presented in Figure 6.4 (the upper two graphs) show clearly that the oxygen interstitial mechanism is favoured, whatever the dopant cation radius. This

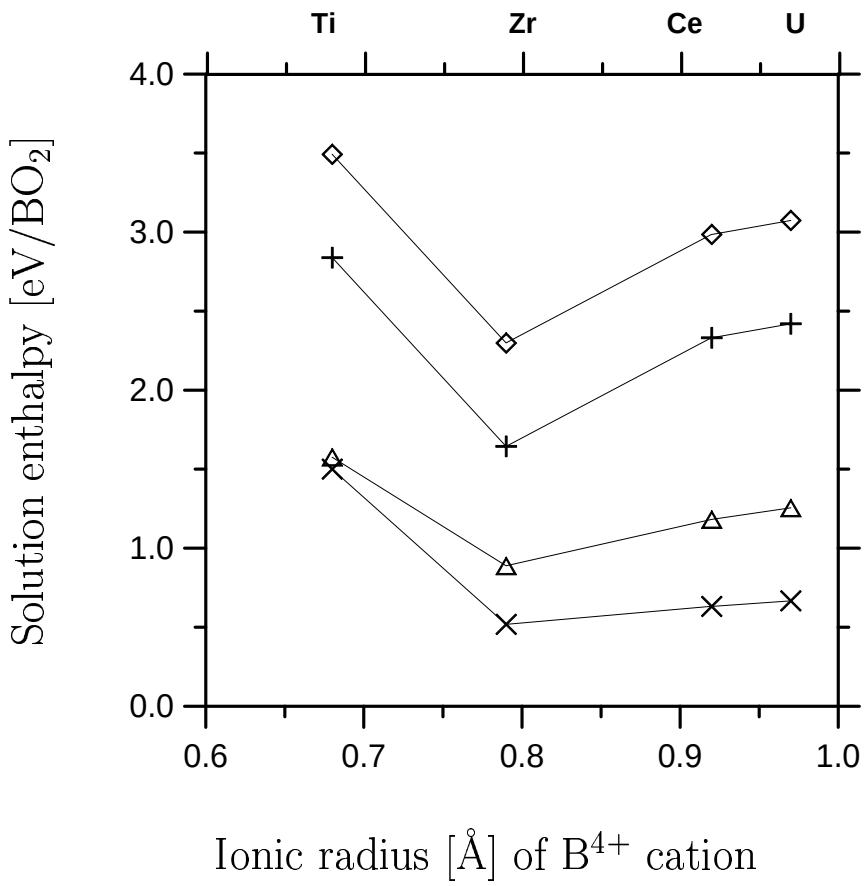

Figure 6.4: Solution of BO_2 oxides in Y_2O_3 . The top two plots assume spatially isolated defects, the bottom two plots solution via the formation of neutral defect clusters: $+$ and $\times$ are for mechanism I (ie. compensation by O_i''), $\diamond$ and $\triangle$ for mechanism II (ie. compensation by V_Y''').

lack of dopant cation influence on solution mechanism preference is not surprising since these two mechanisms are differentiated only by the formation of intrinsic defects (ie. O_i'' or V_Y'''). Consequently, since the oxygen Frenkel reaction is of a lower energy than the Schottky reaction, it follows that for B^{4+} solution, the O_i'' compensation mechanism will be favoured.

With the above reactions, neutral clusters can be formed, either incorporating an oxygen interstitial and two B^{4+} substitutional ions (reaction Ia) or a yttrium vacancy and three B^{4+} substitutional ions (reaction IIa):

$$Ia. \qquad BO_{2(s)} \overset{Y_2O_3}{\rightarrow} \frac{1}{2}\{2B_Y^{\bullet} : O_i''\}^{\times} + \frac{1}{2}Y_2O_{3(s)}$$

$$IIa. \qquad BO_{2(s)} \overset{Y_2O_3}{\rightarrow} \frac{1}{3}\{3B_Y^{\bullet} : V_Y'''\}^{\times} + \frac{2}{3}Y_2O_{3(s)}$$

Both types of clusters can be constructed in different ways. Oxygen interstitial compensated clusters were considered, corresponding to various configurations of the two $B_Y^{\bullet}$ ions, arranged around an O_i'' interstitial ion at the $8b$, $16c$ or $24d$ positions. In this regard, the coordination of the surrounding cations is different for these three interstitial sites: distorted octahedral for $8b$ and $24d$ and distorted tetrahedral for $16c$. We expect cluster defect geometries with a low value of the electric dipole to be favoured.

For the octahedral clusters we can form linear configurations ($B_Y^{\bullet} - O_i'' - B_Y^{\bullet}$) in three orthogonal directions. For the distorted tetrahedral case there are a maximum of 6 possible configurations, yielding solution enthalpy differences as large as 3 eV. Of all these different possibilities the preferred solution cluster is centered around an oxygen interstitial in the octahedral $16c$ site, with one exception; Zr^{4+} prefers to occupy a cluster centered at a $24d$ site.

Clusters incorporating a yttrium vacancy were investigated for configurations centered at $8a$ and $24d$ lattice positions. In these clusters defect ions are further

apart than in the oxygen interstitial compensated clusters. The yttrium vacancy compensation reaction requires three metal substitution sites and a central yttrium vacancy. When the vacancy is at a $8a$ site, there are 10 possible nearest neighbour metal sites for the B^{4+} ions to occupy. Consequently it is possible to form a cluster in which all ions are in one plane, minimizing the electric dipole of the cluster. For the cluster centered at a $24d$ site there are 12 possible cation sites for B^{4+} ions leading to some variety of complex cluster geometries. Nevertheless, we predict that the most stable clusters are centered at the $8a$ yttrium vacancy. This cluster centre is preferred by approximately 0.5 eV over all $16c$ configurations, what ever the dopant cation.

The effect of defect cluster formation on solution enthalpy can be seen by comparing the top two plots in Figure 6.4 with the bottom two. From this it is clear that for small cations (ie. Ti^{4+} and Zr^{4+}) the binding energy associated with the yttrium vacancy (V_Y''') is significantly greater than that associated with the oxygen interstitial (O_i''). The difference in binding energy is sufficiently great that for Ti^{4+} solution the energies associated with both mechanisms become almost the same. Conversely, for larger cations the binding energies are similar so that the oxygen interstitial solution mechanism remains clearly dominant.

Thus overall, we find that the solution enthalpy is a strong function of the 4+ dopant cation radius. Furthermore although oxygen interstitial compensation is always favoured, the extent of its dominance over yttrium vacancy compensation is also a strong function of solute cation radius if we assume that clusters form.

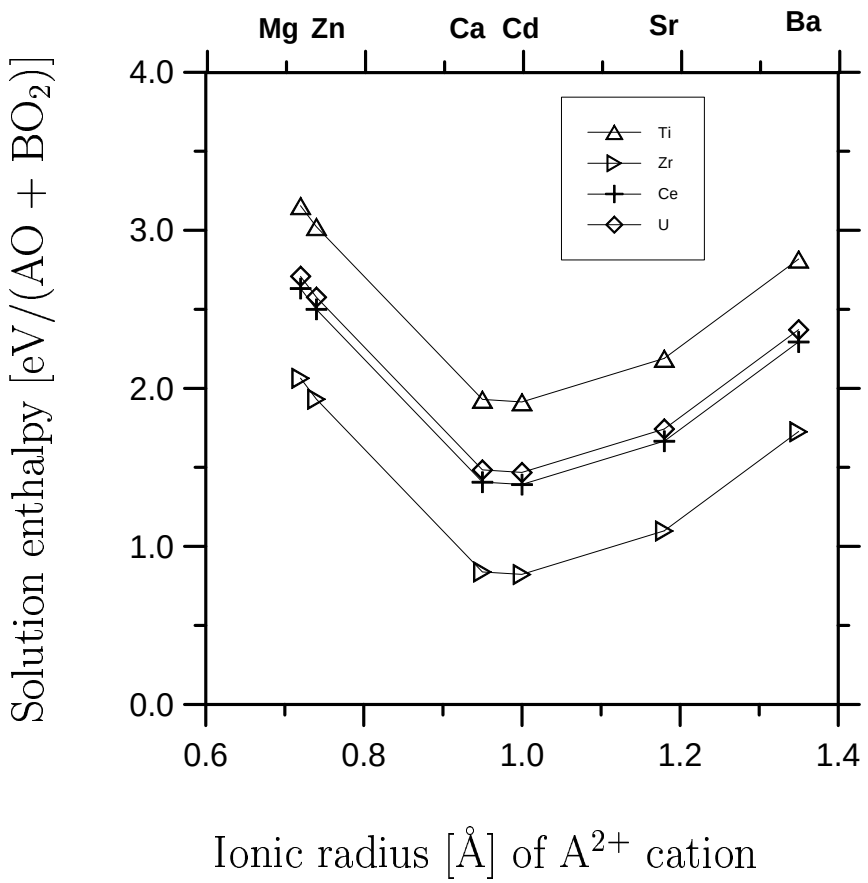

Figure 6.5: The solution enthalpies of equal amounts of BO_2 and AO type oxides, assuming that both substitutional cations are spatially isolated. Each graph corresponds to a B^{4+} cation in co-solution with the series of A^{2+} cations.

6.3.5 Co-doping solution mechanisms

Since in real materials different impurity ions are often present at the same time, as a first step towards understanding multiple dopant ion effects, co-doping solution mechanisms have been studied. The most obvious co-doping mechanism involves equal proportions of AO and BO_2 where the A^{2+} and B^{4+} ions occupy neighbouring yttrium sites.

Figure 6.5 shows the results of co-doping each of MgO, ZnO, CdO, CaO, SrO

and BaO in turn with TiO_2, ZrO_2, CeO_2 and UO_2 but assuming that the charge compensating pairs are spatially isolated. The results are presented as a function of the A^{2+} ionic radii. The minimum solution enthalpy for each of the charge compensating 4+ cations occurs around the radius of Ca. This is not surprising as it is also the minimum point for reaction mechanisms associated with solution of AO oxides via oxygen vacancy (or interstitial) compensation (as in Figure 6.2).

In addition it is also possible to comment on the relative ease of solution of AO oxides via oxygen vacancy or interstitial compensation mechanisms compared to the present co-solution mechanisms. Thus, comparison of Figures 6.2 and 6.5 shows that solution of A^{2+} ions via ZrO_2 and to a minor extent CeO_2 and UO_2 does yield lower solution enthalpies but solution via TiO_2 actually results in a higher energy process.

An important conclusion can therefore be made. Co-solution of A^{2+} and B^{4+} ions does not necessarily imply a greater solubility of A^{2+} despite the fact that with co-solution lattice vacancies or interstitials need not be formed.

The reason for this lies with the high stability of the TiO_2 lattice.

Now let us consider the opposite view, that is, does the solution of B^{4+} ions via charge compensating A^{2+} ions result a lower energy process compared to solution of B^{4+} via oxygen interstitial ions? The answer can be determined by comparing the lower of the top two plots of Figure 6.4 (i.e. for isolated O_i'' compensation) and the minima of each of the four plots in Figure 6.5. In all cases the co-solution mechanism provides a much lower energy mechanism for 4+ cation solution than requiring O_i'' or V_Y'''. However, it is important to bear in mind that although this is always the case for 4+ solution via Cd^{2+}, Ca^{2+} or Sr^{2+} compensation, it is not always the case for Mg^{2+}, Zn^{2+} or Ba^{2+}.

The effect of clustering of the A^{2+} and B^{4+} ions is shown in Figure 6.6. Com-

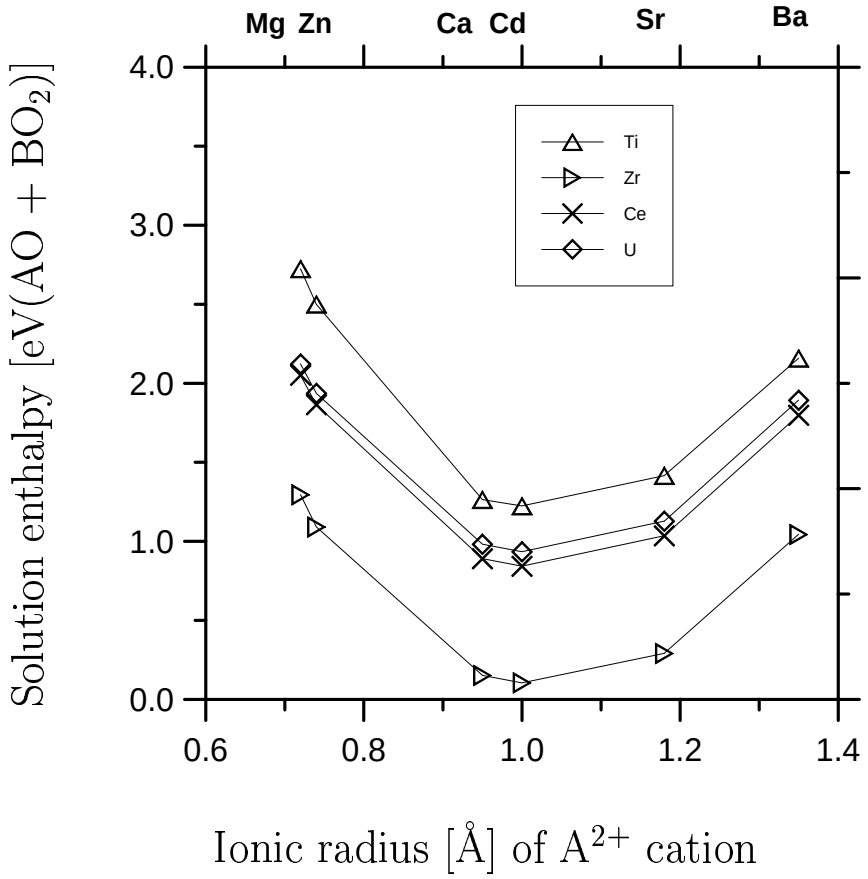

Figure 6.6: The co-solution of BO_2 and AO type oxides. Each graph represents a BO_2 oxide in co-solution with each of the AO type oxides, represented as a function of the A^{2+} ion radius. In all cases, the pairs of cations are in the form of $\{A'_Y : B'_Y\}^{\times}$ neutral defect clusters.

paring Figure 6.6 and 6.5 we immediately see that all solution enthalpies decrease by 0.5-1.0 eV. This is not surprising since the two ions in solution act as mutually compensating defects. However, binding energies associated with A^{2+} and $V_O^{\bullet\bullet}$ or $A_i^{\bullet\bullet}$ and with B^{4+} and O_i'' or V_Y''' are much higher. Therefore, in terms of the solution of B^{4+} ions, defect clustering actually removes the preference for solution of Ce^{4+} and U^{4+} via co-solution with Ca^{2+}, Cd^{2+} or Sr^{2+} rather than via V_Y''' or O_i'' compensation. Thus we predict that co-solution only really aids solution of Zr^{4+} and Ti^{4+}, leading in the case of Zr^{4+} in particular to low solution energies with respect to AO and ZrO_2.

The analysis we have just made is the most simple way of illuminating a number of important points, in particular, that co-solution does not necessarily result in lower solution energies. However, we have assumed that solution occurs for AO and BO_2 oxides. This will not always be true.

6.3.6 Ternary oxides

In the last section, we considered co-solution relative to AO and BO_2 oxides. Here we extend this and calculate solution mechanisms relative to the appropriate ABO_3 oxide *if* the reaction $AO + BO_2 \rightarrow ABO_3$ is predicted to be exothermic. The overall solution reaction becomes:

$$\left.\begin{array}{ll} \text{Components} & AO_{(s)} + BO_{2,(s)} \\ \text{Ternary} & ABO_{3,(s)} \end{array}\right\} \overset{Y_2O_3}{\rightarrow} \{A_Y' : B_Y^{\bullet}\}^{\times} + Y_2O_{3,(s)} \qquad (6.3)$$

as we are assuming solution to the neutral defect cluster. The results are presented in Figure 6.7.

The majority of the ABO_3 compounds investigated were stable, being cubic, or distorted perovskites. Of particular importance is that the Ca, Cd and Sr compounds

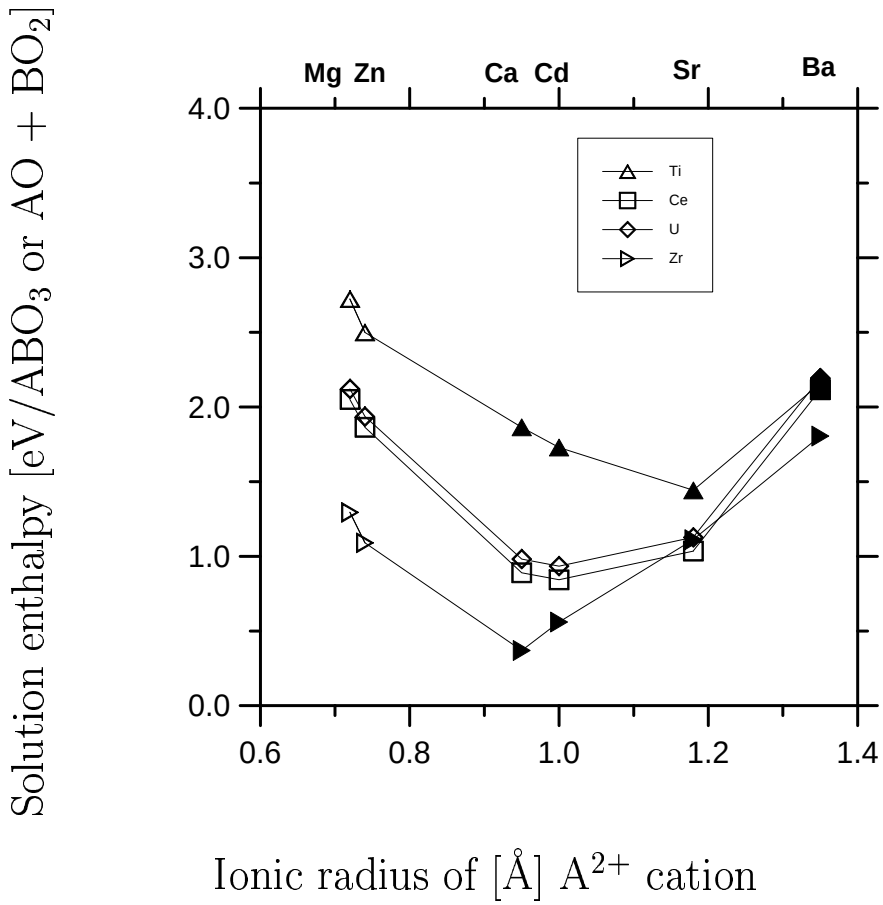

Figure 6.7: The solution enthalpies of the co-solution mechanism where the solution enthalpy is calculated relative to either the ABO_3 ternary oxide (represented as filled symbols) or the respective AO and BO_2 oxides (shown as open symbols), depending on if the ABO_3 compound is calculated to be stable with respect to AO+BO_2.

of Zr and Ti were stable which made the co-solution enthalpies associated with the combinations much less stable. Thus finally it seems that only Ca and Cd co-solution with Ti and Zr exhibit lower solution enthalpies than for the reaction associated with the solution of only 4+ ions. However, even the solution enthalpies of $CaO+ZrO_2$ and $CdO+ZrO_2$ were increased when considering solution with respect to the appropriate ternary oxide (i.e. the ternary oxide was stable). Nevertheless, as Figure 6.7 testifies, significant solubility of these materials in Y_2O_3 should still be expected.

6.4 Concluding comments

In the Y_2O_3 lattice atomic transport will be controlled by the absolute concentrations of defects such as cation and anion vacancies and interstitials. These can be introduced into the lattice by doping with aliovalent impurities. The work we have carried out predicts that the solution energies of a variety of such dopant ions vary greatly with the radius of the dopant cation. Furthermore, even the lowest energy mechanism for solution and hence the corresponding charge compensating defect is a function of cation radius. Thus as cation radius is changed, the relative proportion of different charge compensating defects should change dramatically. This effect is greater for 2+ dopant ions than for 4+ dopant ions. The situation is further complicated by co-solution mechanisms in which the 2+ and 4+ ions are charge self-compensating and by the possibility of forming ABO_3 ternary oxides. Despite the complexities, atomistic computer simulation can be used to provide a consistent set of energies from which it is possible to develop an understanding of the system. Some general comments can be made based on these relative energies while avoiding

having to rely on absolute energies.

- For isovalent solution, the two host lattice cation sites give rise to almost identical solution site energies.

- For AO monoxide solution, small radius cations show a strong preference for dopant interstitial compensation (i.e. by $A_i^{\bullet\bullet}$) while for large cations charge compensation by oxygen vacancies or dopant interstitial compensation is energetically equivalent. If defect clustering is included in the model, charge compensation of large cations is predicted to be via oxygen vacancies.

- Defect cluster binding energies are generally large due to the unusually low static dielectric constant of Y_2O_3 .

- For BO_2 dioxide solution the oxygen interstitial compensated mechanism is dominant whether defect clustering is included or not.

- The co-solution enthalpies associated with mutual charge compensating $A_Y^{'}$ and $B_Y^{\bullet}$ defects, though sometimes low and lowered further by the formation of neutral $\{A_Y^{2+} : B_Y^{4+}\}^{\times}$ pairs, does not usually result in lower solution enthalpies than the solution of AO or BO_2 alone. This is due to the high stability of the AO, BO_2 and ABO_3 oxide lattices. The exception to this involves Ca^{2+} or Cd^{2+} with Zr^{4+} or Ti^{4+} but only solution via Zr^{4+} actually leads to what might be considered low solution enthalpies.

- Solution enthalpies are usually considerably lower than enthalpies for Schottky and Frenkel disorder indicating that vacancy and interstitial lattice ion concentrations will be due primarily to impurity compensation, that is extrinsic processes.

- In general, since we assume a fully ionic model and calculations correspond to the dilute limit, defect enthalpies will be overestimated. Nevertheless, relative energies are very reliable. Therefore, any use of these absolute predicted energies should be made with caution.

Part III

Molecular Dynamics